Particuology 115 (2026) 55–67

Contents lists available at ScienceDirect

Particuology

journal homepage: www.elsevier.com/locate/partic

Laser ignition and combustion process of single boron agglomerate in steam

Gan Yang[a], Binbin Chen[a,*], Likun Ma[a], Yunchao Feng[a], Lian Duan[b], Zhixun Xia[a], Chaolong Li[c]

[a] Advanced Propulsion Technology Laboratory, National University of Defense Technology, Changsha, 410073, China
[b] School of Mechanical Engineering and Mechanics, Xiangtan University, Xiangtan, 411105, China
[c] Test Center, National University of Defense Technology, Xi'an, 710106, China

HIGHLIGHTS

- A single-particle laser ignition system is established to study boron combustion in steam.
- Boron agglomerates in steam undergo four distinct combustion stages.
- Steam triggers a unique micro-explosion mode with sustained jetting rather than expansion.
- Quasi-steady combustion in steam is diffusion-controlled with a rate constant comparable to air.
- Boron achieves ~39.1% combustion efficiency in pure steam, confirming its potential as oxidizer.

GRAPHICAL ABSTRACT

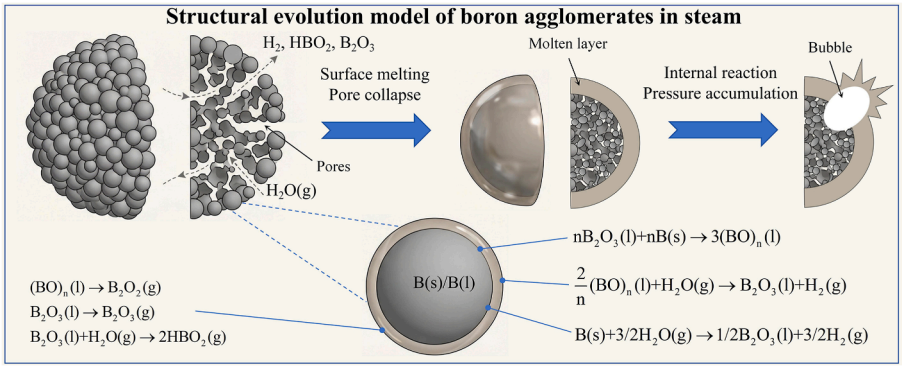

ARTICLE INFO

Keywords:
Boron agglomerate
Laser ignition
Steam atmosphere
Micro-explosion
Combustion kinetics
Single particle

ABSTRACT

To investigate the ignition and combustion mechanisms of boron agglomerates in oxygen-free steam for water ramjet applications, a laser ignition single-particle experimental system was established. The combustion process was found to comprise four sequential stages: preheating and structural loosening, molten collapse, micro-explosion combustion, and quasi-steady combustion. The results indicate that steam can act as an oxidizer to support vigorous boron combustion. Its unique chemical role (reacting with B_2O_3 to form volatile HBO_2) effectively accelerates the removal of the surface oxide layer, resulting in a relatively thin molten shell. Entrapped steam continuously reacts with internal boron, generating gaseous products (H_2, etc.) that trigger a distinct micro-explosion mode characterized by sustained ejection rather than the expansion-dominated behavior observed in air. Kinetic analysis reveals that the quasi-steady combustion stage is diffusion-controlled, with a burning rate constant comparable to that in air. A quantitative evaluation based on volume change yields a final combustion efficiency of approximately 39.1% in pure steam. These single-particle-level observations provide essential experimental evidence for understanding boron combustion mechanisms and for designing boron-based water-reactive fuel systems.

* Corresponding author.
E-mail address: chenbinbin11@nudt.edu.cn (B. Chen).

https://doi.org/10.1016/j.partic.2026.05.007
Received 2 March 2026; Received in revised form 23 April 2026; Accepted 5 May 2026
Available online 20 May 2026

1. Introduction

Boron (B) is regarded as a highly promising high-energy-density fuel in the fields of propulsion and energy due to its exceptionally high mass calorific value (58.9 kJ/g) and volumetric calorific value (137.8 kJ/cm^3) (Song et al., 2021). The reaction between boron and water (B-H_2O) not only releases substantial heat but also generates hydrogen gas, with up to 277 g of hydrogen produced per kilogram of boron via hydrolysis (Rohani et al., 2016). This enables the dual conversion of chemical energy into both thermal energy and hydrogen energy (Vishnevetsky et al., 2008; Wahbeh et al., 2012, 2013). This characteristic gives boron unique advantages in energy systems such as hydrogen production via hydrolysis and water ramjet. Particularly in scenarios like underwater propulsion or distributed power supply for subsea equipment, using water as an in-situ oxidizer can significantly simplify system design and enhance energy density.

For a long time, research on boron combustion has primarily focused on its ignition and combustion mechanisms in air or oxygen environments, and the corresponding models are relatively well established (Hussmann & Pfitzner, 2010a, 2010b; Liang et al., 2018, 2021; Wu & Wei, 2024). Boron exhibits a two-stage combustion process consisting of ignition and combustion phases. During the ignition stage, a liquid oxide layer exists on the particle surface, and the reaction is limited by the diffusion of components within this layer. In the combustion stage, the oxide layer is essentially removed, representing a fundamental difference in reaction mechanisms between the two stages. Numerous studies have demonstrated that the presence of water vapor can significantly enhance the combustion of boron particles in oxygen-containing atmospheres. The primary mechanism is that water vapor can react with the liquid boron oxide (B_2O_3) on the particle surface to form volatile species (e.g., HBO_2), thereby accelerating the removal of the oxide layer, lowering the ignition temperature, and shortening the ignition delay time (Brown et al., 1991; Gaponenko et al., 1981; Liang et al., 2021; Liu et al., 2024).

On the other hand, research focusing on the boron-water reaction itself has predominantly concentrated on the non-combustion hydrolysis process for hydrogen generation within the low to medium temperature range (typically below 1000 K) (Rosenband et al., 1998; Vishnevetsky et al., 2008). These studies aim to utilize boron's potential for chemical hydrogen production through methods such as boron nano-preparation, photocatalysis, and catalysts (e.g., Ni, NaH) (Majji et al., 2024; Meera et al., 2022; Rohani et al., 2016; Zhang et al., 2021). These approaches enable boron to react with water under mild conditions, but the particle temperature remains low throughout the process without removing the liquid oxide layer—that is, without entering the combustion stage. The reaction rate is diffusion-controlled through the liquid oxide layer, resulting in a slow process with a low energy release rate, which struggles to meet the application demands of underwater power systems for rapid and high-intensity energy release. Consequently, there is a lack of systematic experimental research on the entire ignition and combustion process of boron in oxygen-free or oxygen-lean steam environments, particularly under high-temperature, high-heat-flux conditions simulating engine operating states. This knowledge gap hinders the accurate understanding and optimization of the real physicochemical processes inside the combustion chamber of boron-based water ramjet.

Furthermore, in practical applications, particularly on the surface of boron-containing fuel-rich propellants and within low-speed recirculation zones of combustion chambers, amorphous boron particles initially at the micrometer scale are prone to agglomeration, forming agglomerates with sizes ranging from tens to hundreds of micrometers (Qu et al., 2025). This agglomeration behavior significantly alters the heat and mass transfer characteristics, reaction pathways, and combustion stability of the particles, and can lead to special combustion phenomena such as micro-explosions (Duan et al., 2023; 2024; Mi et al., 2013). Therefore, investigating the combustion behavior of boron agglomerates is crucial for understanding the energy release patterns in real systems. Additionally, the larger size of the agglomerates facilitates high-resolution observation at the single-particle level, enabling precise capture of subtle phenomena—such as structural evolution, stage transitions during combustion, and potential micro-explosions—without interference from neighboring particles.

Therefore, to clarify the combustion behavior of boron in steam and reveal its energy release characteristics under conditions close to actual engine operation, this paper employs a laser ignition experimental method to conduct an in-depth study on the ignition and combustion process of a stationary single boron agglomerate in a steam environment. Laser ignition technology can provide an extremely high heating rate, effectively simulating the high heat flux conditions within an engine. Simultaneously, its precise spatial positioning allows the particle to remain stationary, eliminating the effects of particle movement and mutual interference, thereby enabling "clean" observation of single-particle combustion behavior. By creating a controlled steam atmosphere, this study aims to directly observe the laser ignition and combustion process of boron agglomerates in steam, and to explore their special combustion behaviors (such as the generation and role of micro-explosions) and kinetic characteristics. It should be noted that pure steam was selected as the experimental atmosphere in this study as a simplified yet scientifically justified abstraction of the actual environment in a water ramjet combustion chamber. Under practical operating conditions, the secondary combustion chamber also contains primary combustion products such as CO and H_2. However, steam serves as the predominant oxidizer governing the subsequent combustion behavior of boron particles. The use of a pure steam atmosphere effectively eliminates interference from other species, thereby enabling precise characterization of the intrinsic reaction kinetics between boron and water. The research findings will provide crucial theoretical foundations and experimental support for the fuel design, combustion organization optimization, and performance prediction of boron-based water ramjets.

2. Material and methods

2.1. Material characterization

The boron agglomerate particles used in this study were prepared from commercially available amorphous boron powder via the spray granulation method. This method allows for the production of spherical agglomerate particles with controlled size and morphology, which facilitates experimental reproducibility. Chemical purity analysis was conducted on the agglomerates to determine their composition. The primary impurities were oxygen (O) and magnesium (Mg). The mass fraction of oxygen, measured using an oxygen/nitrogen analyzer, was 5.18%. The mass fraction of magnesium, measured using Inductively Coupled Plasma Optical Emission Spectroscopy (ICP-OES), was 2.21%. The particle size distribution was obtained via wet dispersion (using ethanol as the dispersant) with a Malvern Mastersizer 2000 laser particle size analyzer. Detailed results of the chemical composition and particle size distribution are provided in Section S1 of the Supplementary Material. To facilitate clear observation of single-particle combustion behavior, boron agglomerates with diameters of 350–450 μm were selected for experiments. Average values from multiple repeated trials were used in quantitative analysis to mitigate the influence of initial particle size variations. The surface morphology and microstructure of the agglomerates were observed using scanning electron microscopy (SEM). As shown in Fig. 1, the agglomerates exhibit a typical porous structure formed by the physical accumulation of numerous primary amorphous boron particles (approximately 1 μm in size). The porosity of the agglomerate particles, measured using the Archimedes method, was 48.9 ± 5%.

2.2. Experimental system and parameter settings

To investigate the ignition and combustion characteristics of a single

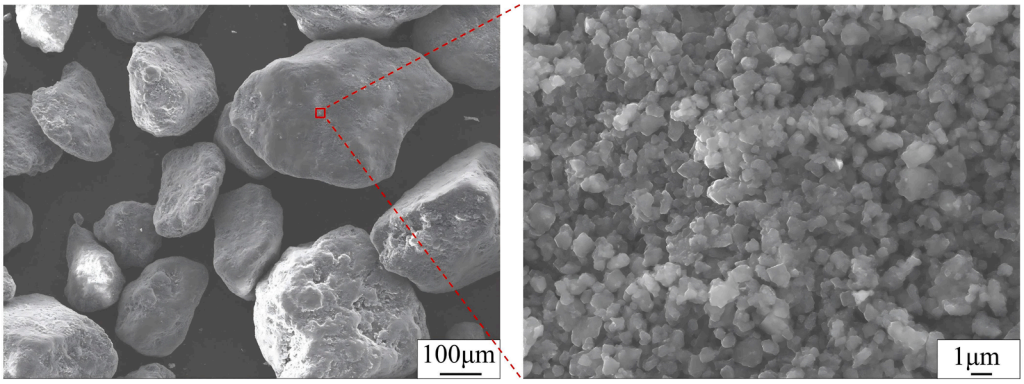

Fig. 1. Surface morphology of the boron agglomerates.

boron agglomerate in steam, a dedicated experimental system for laser ignition combustion was constructed. The system primarily consists of three core modules: the laser ignition module, the atmosphere conditioning module, and the combustion diagnostics module. These modules are synchronized via a controller to achieve precise timing coordination. The overall layout of the experimental system is shown in Fig. 2(a).

The laser ignition module utilizes a continuous-wave fiber laser (wavelength 1080 ± 10 nm, maximum output power 255 W). A single boron agglomerate was placed on a tungsten disc mounted on the sample stage within the sealed combustion chamber. The laser beam was vertically incident from above, passing through a fused silica window, with a laser spot approximately 3 mm in diameter fully covering the target particle. Prior to experiments, a laser power meter (Ophir, F150A-BB-26) was used to precisely measure and calibrate the actual laser power reaching the particle surface after attenuation by the window and the atmosphere, ensuring consistent heating conditions. Experiments were conducted at three laser power densities: 12.13, 16.46, and 21.55 W/mm^2. This paper primarily presents the combustion process observed under the 16.46 W/mm^2 condition as an example. The laser duration for all experiments was set to 500 ms to ensure the particles underwent complete heating, ignition, and combustion processes.

The core challenge of the atmosphere conditioning module lies in achieving a stable, pure, and condensation-free high-temperature steam environment. Since water vapor readily condenses under standard temperature and pressure, a series of special designs were implemented in this system. First, fiberglass heating tapes were wound around the combustion chamber shell and all gas lines, and the entire system was preheated to 400 K prior to experiments. At this temperature, the saturated vapor pressure of water is approximately 0.25 MPa (Fig. 3), allowing for the establishment of a pure steam atmosphere inside the

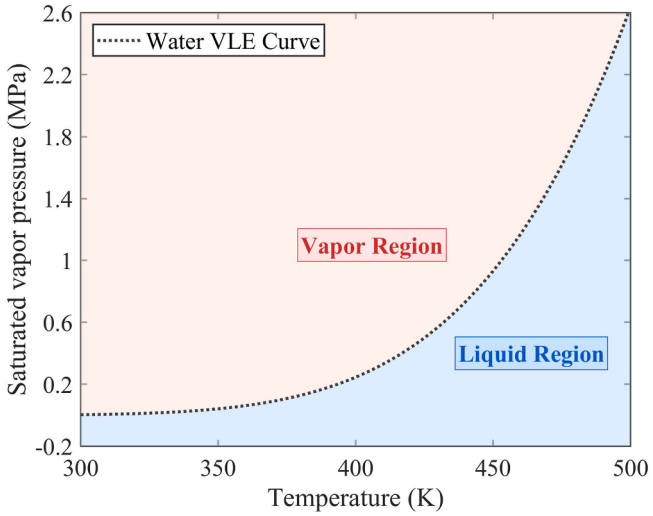

Fig. 3. Saturated vapor pressure of water at different temperatures.

combustion chamber at pressures up to 0.25 MPa. An independent heating device was installed at the quartz observation window to prevent local condensation from affecting optical observations. To ensure atmosphere purity, the combustion chamber was initially evacuated using a vacuum pump, then filled with high-purity argon; this cycle was repeated three times to thoroughly eliminate air interference. Finally, after another evacuation, superheated steam generated by an electric steam generator (Yike, YK-SPG01) was introduced into the combustion

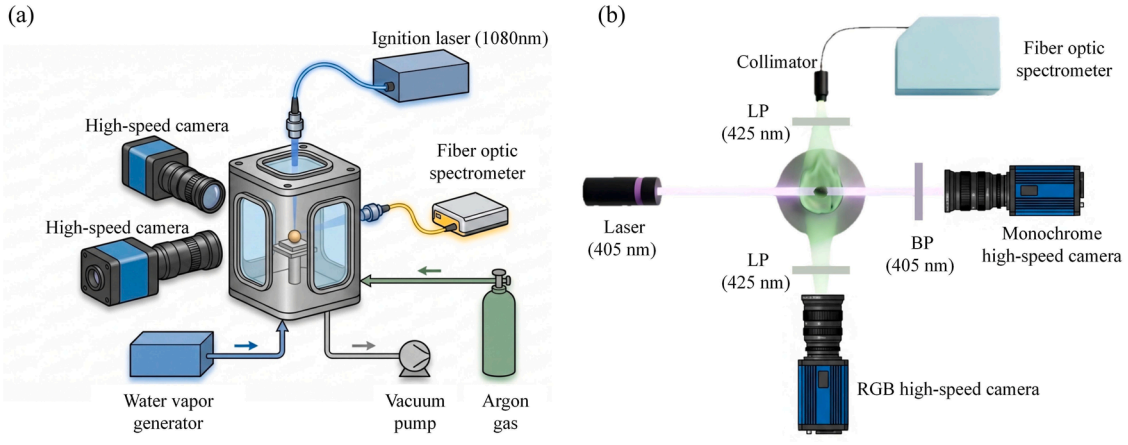

Fig. 2. Schematic of experimental system: (a) Overall layout; (b) Optical path of the combustion diagnosis module (BP: bandpass filter; LP: longpass filter).

chamber. When the pressure reached the set value, the intake valve was closed and the laser ignition was immediately triggered. In addition to steam, laser ignition experiments in dry air and argon were also conducted as controls to compare the combustion behavior of boron agglomerates in these three atmospheres. All experiments were performed at an ambient pressure of 0.1 MPa. Although argon and air do not present condensation issues, the combustion chamber was still preheated to the same temperature (400 K) to eliminate the influence of initial environmental temperature differences on the particle heating process, ensuring that the comparison of combustion characteristics was based on the same thermal starting point.

The combustion diagnostics module employs a multi-angle, multi-device synchronous observation strategy to comprehensively capture details of the combustion process (a schematic diagram is shown in Fig. 2(b)). Specifically, a monochrome high-speed camera (PCO, dimax HS4), combined with a 405 nm semiconductor laser and a corresponding narrowband filter, was used for shadowgraph imaging to record the particle's projected profile from one side. This wavelength band avoids the major characteristic radiation and intense thermal radiation from boron combustion, thus clearly revealing structural evolution, volume changes, and potential phenomena such as expansion and fragmentation of the particle itself. On the other hand, a color high-speed camera (PCO, dimax S4) was used to record the incandescence emission images of the combustion process from another viewing angle. A 425 nm longpass filter was installed in front of its lens to block interference from the 405 nm laser; the filter's transmittance decays beyond 900 nm, thereby also blocking interference from the 1080 nm ignition laser. The frame rates of both high-speed cameras were set to 4000 fps, enabling the capture of transient processes with a temporal resolution of 0.25 ms. Furthermore, after synchronized triggering, the images captured by the two cameras correspond precisely in time, facilitating subsequent comparative analysis. Simultaneously, a fiber-optic spectrometer (Ocean Optics, HR2000+ES) was used to monitor the spectral evolution during combustion. The integration time of the spectrometer was set to 2 ms. A collimating lens with a diameter of 5 mm was attached to the end of the optical fiber, and a 425 nm longpass filter was also added to filter out the laser and avoid saturation. Prior to experiments, the spectrometer was intensity-calibrated using a standard tungsten halogen light source (Ocean Optics LS-1-CAL).

2.3. Data processing methods

2.3.1. Area calculation based on images

In addition to providing an intuitive understanding of the particle's ignition and combustion process, area information reflecting different physical processes is primarily obtained through image processing based on the two types of images acquired from the high-speed cameras.

Shadowgraph images exclude interference from combustion luminescence and thermal radiation, allowing clearer observation of the particle's own morphological evolution and structural fragmentation. The projected area of the particle, derived from shadowgraph images, represents the region where the particle body blocks the background light, more accurately reflecting changes in the particle's size and shape during combustion.

The luminous zone area can be obtained from the incandescence emission images. This area encompasses the thermal radiation from the high-temperature particle surface, the surrounding gaseous combustion flame, and any luminous regions from ejected material. It reflects the overall intensity and spatial extent of the combustion reaction.

2.3.2. Particle temperature calculation based on spectral data

According to Planck's law, particles exhibit different thermal radiation spectra at different temperatures. Therefore, the surface temperature of a particle can be inverted and calculated based on spectral data. Specifically, the multi-wavelength fitting method is employed (Mi et al., 2013). This method utilizes spectral intensity data across multiple wavelengths within a broad band to jointly solve for the temperature, offering higher stability and accuracy compared to the two-color pyrometry method. The measured spectral radiation intensity $I(\lambda)$ at wavelength λ can be expressed as:

$$I(\lambda) = \varepsilon(\lambda) \cdot \frac{C_1 \cdot \lambda^{-5}}{\exp\left(\frac{C_2}{\lambda T}\right) - 1} \tag{1}$$

where $\varepsilon(\lambda)$ is the spectral emissivity of the boron particle surface; C_1 and C_2 are the first and second radiation constants, respectively; and T is the particle surface temperature (K). Within the visible spectrum, where $C_2/\lambda T$ is sufficiently large, Wien's approximation can be applied, and the above equation can be linearized as:

$$\ln\left[I(\lambda) \cdot \lambda^5\right] = -\frac{C_2}{\lambda} \cdot \frac{1}{T} + \ln[\varepsilon(\lambda) C_1] \tag{2}$$

By plotting $1/\lambda$ on the horizontal axis and $\ln\left[I(\lambda) \cdot \lambda^5\right]$ on the vertical axis for linear fitting, the slope of the fitted line is $k = -C_2/T$, from which the temperature $T = -C_2/k$ can be calculated. The intercept term contains emissivity information, which is constant under the gray body assumption and does not affect the slope calculation. Within the 600–800 nm wavelength range, the characteristic emission peaks of intermediate gaseous products from boron combustion are relatively weak, and continuous thermal radiation dominates. Therefore, spectral intensities between 600 and 800 nm were used for fitting (see Supplementary Material Section S2).

Since spectral intensity is sensitive to temperature, the measurement results primarily reflect the temperature information of the hottest radiation source along the optical path. The boiling point of boron is as high as 4200 K, so the boron particle surface is likely the hottest emitter. Consequently, the measurement results are predominantly reflect the surface temperature of the boron particle. When the particle temperature is relatively low, the signal-to-noise ratio of the measured spontaneous emission becomes insufficient for accurate temperature determination. Experimental evaluation indicates that the lower detection limit of this method is approximately 2000 K.

It should be noted that the multi-wavelength fitting method described above relies on the gray-body assumption, i.e., that the spectral emissivity of the particle surface remains constant across the 600–800 nm wavelength range. However, during actual combustion, factors such as scattering by boron oxide smoke and broadband chemiluminescence may cause deviations from gray-body behavior, thereby introducing uncertainties in the temperature inversion. The associated error is estimated to be no greater than ±250 K (Mi et al., 2013). This method provides a reliable means for inversely calculating the surface temperature history of boron agglomerates during combustion.

3. Results and discussion

3.1. Typical ignition and combustion process of boron agglomerates in steam

The ignition and combustion process of a boron agglomerate under laser irradiation exhibits distinct temporal stage characteristics. This section takes the experimental results under a heating power density of 16.46 W/mm^2 as an example to elaborate on the detailed processes and characteristic phenomena of each stage. Fig. 4 shows the variation curves of the projected area and the incandescence area of a typical boron agglomerate (with an equivalent diameter of 451 μm) during the 500 ms laser irradiation period. The entire process can be divided into two main stages: preheating/ignition and combustion, which can be further subdivided into four sub-stages. Overall, the particle volume decreases progressively, but special expansion phenomena occur during two of these sub-stages. Fig. 4(b) and (c) present zoomed-in views of these two sub-stages, respectively.

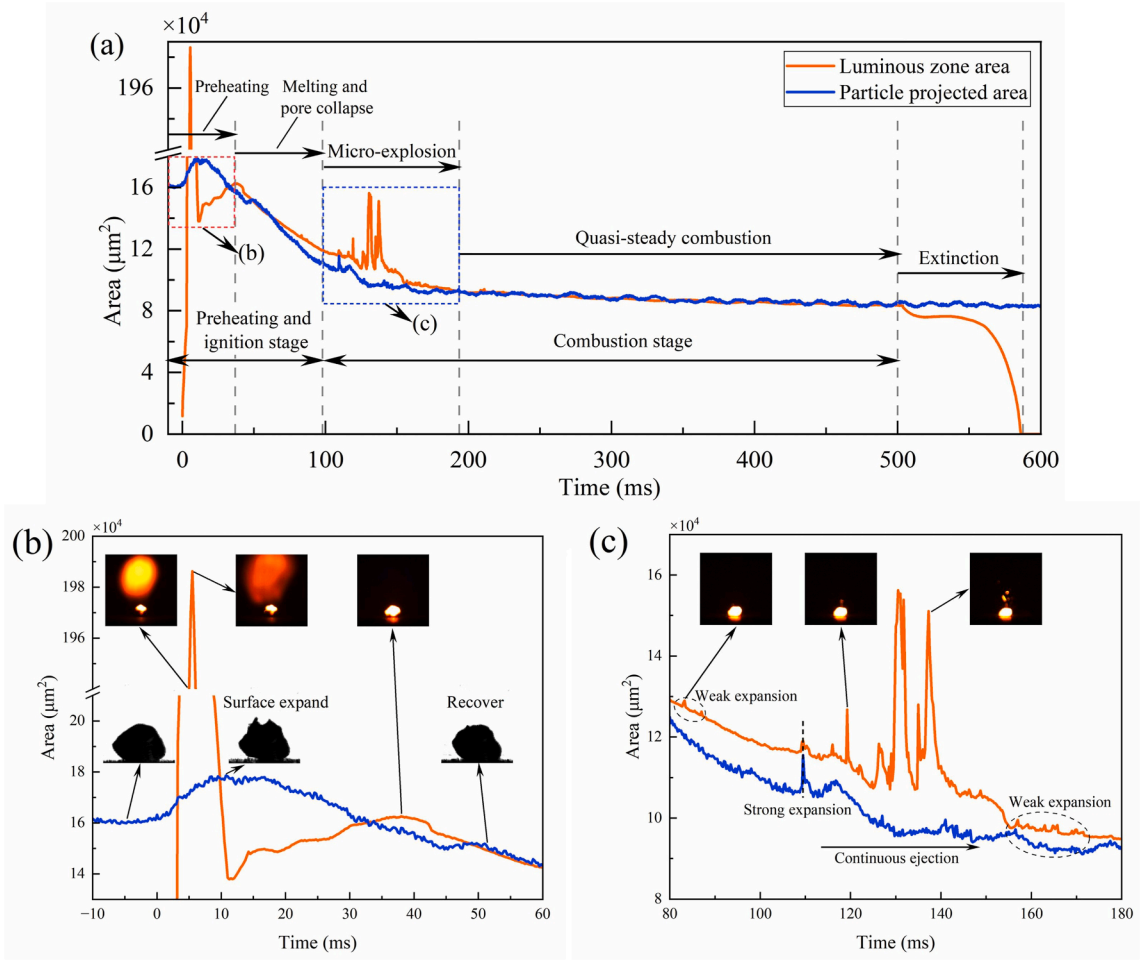

Fig. 4. Temporal evolution of the luminous area and particle projected area in steam: (a) Full duration; (b) Enlarged view of the preheating stage; (c) Enlarged view of the micro-explosion combustion stage.

3.1.1. Preheating and ignition stage

Taking the start of laser irradiation as time zero, the preheating and ignition stage occurs during the initial period of laser action. It is characterized by the rapid input of laser energy, initial disruption of the agglomerate's internal structure, and overall preheating, which creates conditions for subsequent vigorous combustion. Fig. 5 shows the typical structural changes and incandescence phenomena of the boron agglomerate during this stage.

Following laser irradiation, the particle was rapidly heated. Within a few milliseconds, the ejection of fine particles from the particle surface could be observed (Figs. 5 and 1.75 ms), followed by the appearance of a large, transient orange-yellow luminous region above the particle (Figs. 5 and 4.25 ms). This luminous phenomenon was observed in steam, air, and argon atmospheres, occurring within the first 10 ms,

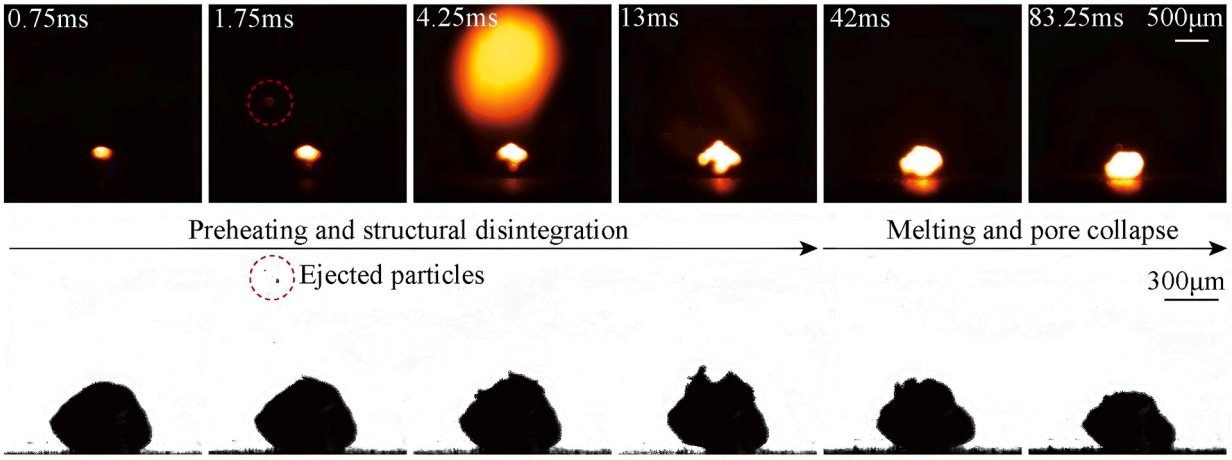

Fig. 5. Images of the boron agglomerate during the preheating and ignition stage in steam (top row: incandescence images; bottom row: corresponding shadowgraphs).

before the particle was sufficiently preheated, indicating it did not originate from boron combustion. Analysis suggests this was caused by the high heat flux of the laser rapidly heating the entrapped gas within the agglomerate's pores, causing it to expand and eject rapidly. The ejected gas stream carried a small number of boron microparticles from the surface; these particles were heated to incandescence within the laser path, forming the observed transient luminosity. The amount of gas within the pores was limited, so this ejection process typically lasted less than 10 ms. The distinct tumbling and rolling of the particle after laser onset, shown in Fig. 6, further confirms the presence of uneven recoil from gas ejection on the surface.

Subsequently, between approximately 8 and 30 ms, noticeable structural loosening of the surface layer occurs. The shadowgraph images (Fig. 5) clearly show the surface becoming rough, with local irregular protrusions or "arm-like" separating structures forming, leading to a slight increase in the projected area (Fig. 4). This phenomenon occurs because the expanding gas ejecting from the interior encounters obstruction from the surface layer. The gas pressure forces the surface layer open, forming arm-like structures that remain connected at one end to the parent particle (Figs. 6 and 4.75 ms). After the internal pressure is released, these protruding structures re-adhere to the particle surface under cohesive forces. This process locally increases the surface porosity and area, loosens the structure, and exposes the inner boron micro-particles to the oxidizing atmosphere, facilitating the adsorption of oxidizers and their diffusion into the particle interior, thereby creating conditions for subsequent reactions.

With continued laser heating, the overall particle temperature rises, and the thermal radiation intensity increases. The luminous area gradually expands from the top until it covers the entire particle surface. When the luminous area reaches its peak, it indicates that the majority of the particle surface has attained a temperature sufficient to emit significant thermal radiation, marking the transition from localized heating to an overall high-temperature state. By this time, the transient gas ejection from the initial preheating stage has ceased, and surface structural changes have largely subsided. The combustion process then enters the melting and pore collapse sub-stage, dominated by surface melting and oxide layer evolution. This stage corresponds to the oxide layer removal process described in classical boron ignition theory.

As shown in Fig. 4, the melting and pore collapse stage occurs roughly between 40 and 100 ms. During this period, both the luminous area and the particle projected area decrease rapidly, and the particle volume reduction rate is the most significant throughout the entire combustion process, indicating that most of the structural densification occurs during this stage. Fig. 5 also clearly shows a noticeable shrinkage in particle volume, and the surface contour becomes smoother and more rounded—a typical characteristic of surface melting.

Fig. 7(a) compares the variation curves of the particle projected area under the three different atmospheres. Notably, even in inert argon (where only physical melting and initial oxide layer volatilization occur), the particle still exhibits significant and similarly rapid volume collapse. This confirms that the primary driving force for volume change in this stage is the physical melting and coalescence of particles, while the chemical exothermic reactions in oxidizing atmospheres primarily serve an accelerating role.

Under the action of surface tension within the high-viscosity molten material, the constituent boron microparticles of the agglomerate coalesce with each other, and the pores gradually close. This leads to a reduction in the agglomerate's size, a decrease in porosity, and the gradual evolution of the initial porous structure into a denser particle morphology. When the surface layer becomes fully molten, a relatively dense liquid film forms on the particle surface, sealing the pores and hindering the escape of internal gas. Consequently, the rate of decrease in the particle projected area slows. Surface closure marks the end of this stage.

At this point, the preheating and ignition stage is complete. Dominated by the input of external laser energy, this stage achieves overall particle preheating, surface melting and densification, and the removal of the surface oxide layer. It results in a non-uniform layered structure characterized by a "sealed surface layer with internal pores still present," thereby creating the conditions for the micro-explosion behavior in the subsequent combustion stage.

3.1.2. *Combustion stage*

Fig. 8 presents typical images of a boron agglomerate during the combustion stage in steam. The agglomerate exhibits significant micro-explosion behavior during this stage, which can be categorized into two types based on the subsequent events: expansion-fracture and expansion-ejection. Shadowgraph imaging captures the expansion and contraction of the particle body (corresponding to expansion-fracture), while incandescence imaging records the expansion of the particle body as well as the incandescent emission from ejected material (corresponding to expansion-ejection). Therefore, sharp peaks in the projected area curve can be used to identify expansion events, while additional peaks in the luminous area curve indicate ejection phenomena.

The enlarged views on the right of Fig. 7 show the particle projected area (a) and luminous area (b) during the micro-explosion stage in the 3 atm. In inert argon, both area curves are relatively smooth, with no significant sharp peaks observed. This indicates that thermal expansion of internal gas and volatilization of initial oxides alone are insufficient to trigger micro-explosions, confirming the necessity of an oxidizing atmosphere. Distinct micro-explosion phenomena are observed in both steam and air, accompanied by continuous particle volume reduction. However, the two modes differ significantly. In air, the projected area curve exhibits multiple sharp peaks (Fig. 7(a)), indicating intense expansion, while the luminous area shows fewer and weaker peaks (Fig. 7(b)), suggesting relatively weak ejection. Conversely, in steam, the luminous area displays several strong peaks (Fig. 7(b)), indicating vigorous and sustained ejection, whereas the projected area presents fewer and smaller peaks (Fig. 7(a)), reflecting weaker expansion. It should be noted that the three curves presented in Fig. 7 were obtained from different particles with slight variations in initial projected area (relative deviation in diameter approximately 8%), and are intended to provide a direct visual comparison of the typical micro-explosion behavior in the 3 atm. In the subsequent quantitative analysis, average values from multiple repeated experiments and normalized

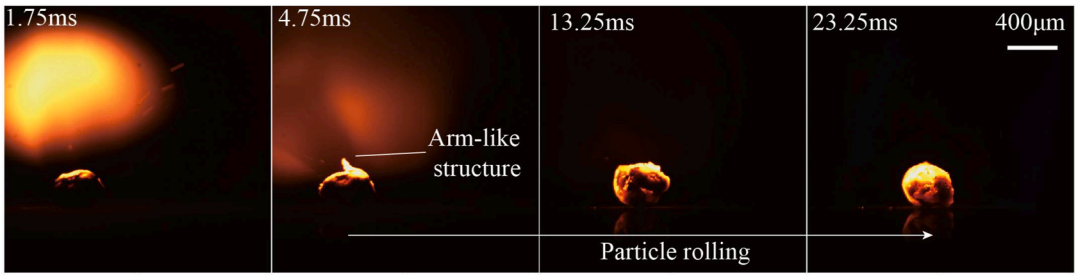

Fig. 6. Structural evolution and particle motion of a boron agglomerate during preheating.

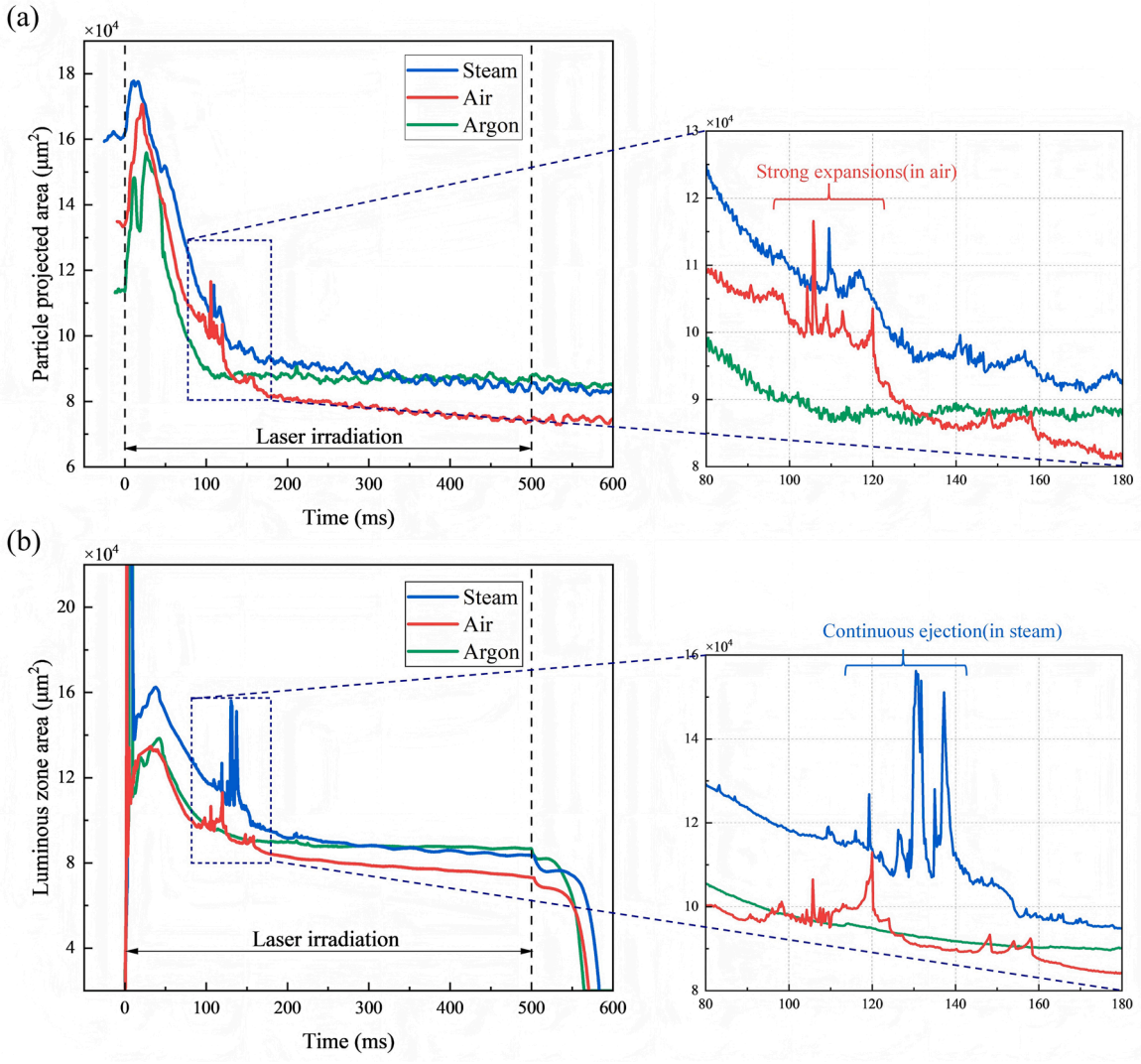

Fig. 7. Temporal evolution of the area in different atmospheres: (a) Particle projected area and its enlarged view during micro-explosion stage; (b) Luminous area and its enlarged view during micro-explosion stage.

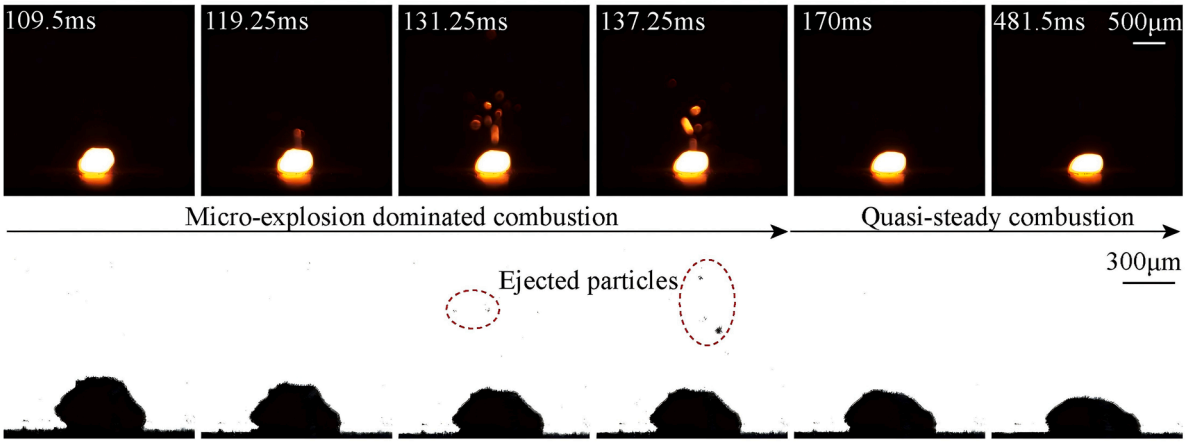

Fig. 8. Images of the boron agglomerate during the combustion stage in steam (top row: incandescence images; bottom row: corresponding shadowgraphs).

variables are employed to eliminate the influence of initial particle size differences. Further statistics on the frequency of expansion and ejection events for particles of varying sizes are provided in the Supplementary Material S3, which confirm the conclusion drawn here: micro-explosions in steam are characterized predominantly by sustained ejection, whereas those in air are dominated by stronger expansion.

This difference stems from variations in surface molten layer thickness and internal gas generation behavior under the two atmospheres.

Strong expansion requires not only gas generation within the particle but also a surface molten layer of sufficient thickness to withstand substantial expansion deformation. Fig. 4(c) compares the evolution of the two types of area curves during micro-explosion combustion stage in steam. Following a strong initial expansion, the boron particle exhibits continuous ejection without significant subsequent expansion, showing only minor high-frequency oscillations. This occurs because, in steam, the heat release from the boron-water reaction is relatively weak, resulting in a slower particle melting rate. Additionally, steam effectively accelerates oxide layer removal, leading to the formation of a thinner surface molten layer. Concurrently, the boron-water reaction has a high gas generation rate (e.g., H_2, HBO_2). After an initial expansion-fracture event, the liquid film of the semi-molten particle cannot promptly repair itself. Consequently, internal gas continuously escapes through the opening in the liquid film, preventing effective pressure buildup. This results in the observed "expansion - sustained ejection" micro-explosion combustion mode.

Fig. 9 visually illustrates the characteristic phenomena of a boron agglomerate during micro-explosion combustion in steam. At 76.25 ms, local expansion occurs at the top of the particle. By 92.75 ms, the expanded region ruptures, initiating ejection. From 92.75 ms to 156.75 ms, ejection persistently occurs at the same location without significant further expansion of the particle. During the ejection process, the incandescence intensity at the center of the particle weakens, forming a dark spot. This phenomenon reflects the diffusion of internal material, which travels through internal pores to the rupture opening at the particle top where ejection takes place. In addition, micro-explosions originating from the bottom of the particle and causing detachment from the substrate were repeatedly observed during the experiments (see Supplementary Material S4 for details). This indicates that despite the directional nature of laser heating, a dense molten layer can form on all sides of the particle, and micro-explosions are not confined to the laser-irradiated surface.

In air, the strongly exothermic boron-oxygen reaction not only accelerates particle melting into the micro-explosion combustion stage but also promotes the formation of a thicker surface molten layer. This thicker layer effectively accumulates internally generated gases (primarily from oxide volatilization) and rapidly reseals after rupture, thereby triggering multiple intense expansions. Simultaneously, the boron-oxygen reaction produces less gas, and the thick molten layer exhibits stronger encapsulation and adhesion of internal microparticles, suppressing material ejection.

Due to the limited amount of gas that can be generated within the inner layers of the particle, after the micro-explosive combustion persists for a period (typically concluding within 200 ms), the expansion and ejection of the particle gradually weaken. The changes in the particle's projected area and luminous zone area tend to plateau (Fig. 4(a)), with the area decreasing slowly and no significant combustion behavior observed (Fig. 8). This phase is therefore referred to as the quasi-steady combustion stage. Even if the laser irradiation time is extended, the particle morphology does not change significantly. This indicates that the internal pores and oxides have been largely removed, and the gas that can be generated inside the particle has reached its limit under this heating power, preventing further accumulation required for micro-explosions. The internal reactions of the particle essentially cease, and the process transitions to oxidation dominated by the particle's external surface.

After the laser irradiation stops, the incandescent emission rapidly decays until it disappears. The period from laser cutoff to the complete disappearance of self-luminescence is defined as the flameout time. As shown in Fig. 7(b), significant differences in flameout time are observed under different atmospheres. The average flameout times in steam, air, and argon are 86.0 ms, 72.5 ms, and 64.3 ms, respectively. The longest flameout time in steam suggests that steam helps sustain surface reactions at lower temperatures, enhancing the particle's self-sustaining combustion capability. This may be related to steam's ability to remove the boron oxide layer.

3.2. Particle surface temperature analysis

Based on the multi-wavelength spectral fitting method, the surface temperature evolution of boron agglomerates in steam, air, and argon atmospheres was inversely derived (Fig. 10). Under all three atmospheres, the particle surface temperature exhibited a trend of rapid increase, reaching a peak, followed by a slow decline. After laser irradiation, the particle surface temperature rapidly rose within 50 ms, exceeding the boiling point of B_2O_3 (approximately 2133 K), indicating rapid melting and vaporization of the surface oxide layer. Subsequently, the temperature was mainly maintained between the boiling point of B_2O_3 and the melting point of crystalline boron (approximately 2350 K). Within this temperature range, amorphous boron gradually softens and melts; therefore, the molten surface layer during the combustion stage primarily consists of liquid boron.

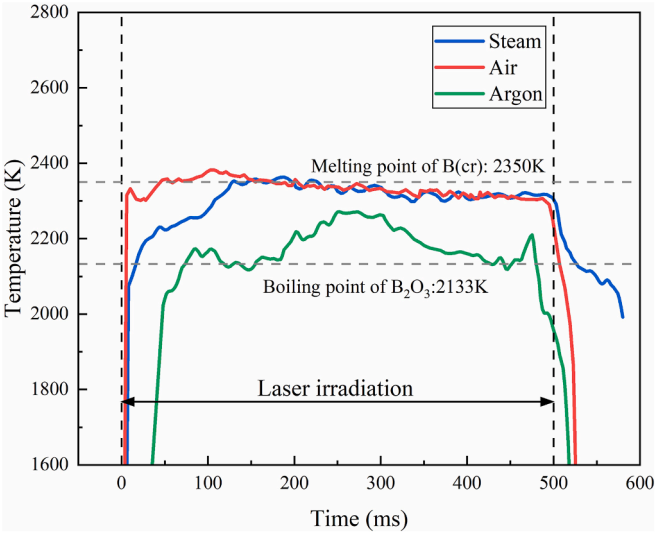

Fig. 10. Evolution of particle surface temperature in different atmospheres.

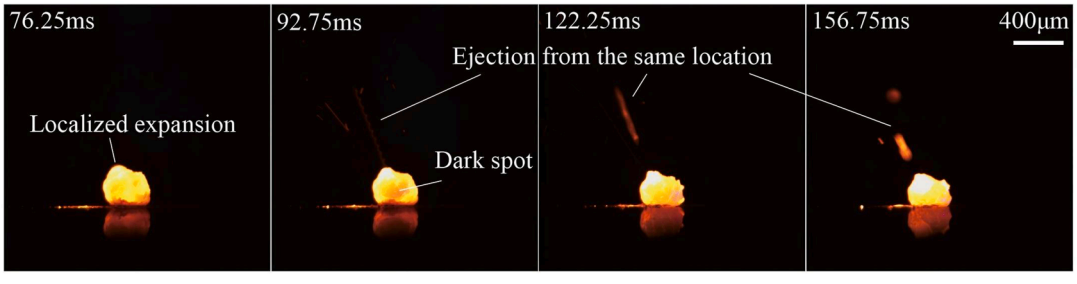

Fig. 9. Characteristic phenomena of a boron agglomerate during micro-explosion in steam.

Comparing the different atmospheres, distinct differences in temperature evolution are observed. In air, the particle surface temperature rises the fastest and remains higher than that in the steam environment until 150 ms. This is related to the higher heat release rate of the boron-oxygen reaction and is consistent with the observations in Section 3.1 of faster molten collapse and earlier micro-explosions in air. The temperature curve in steam rises slightly more slowly but exceeds the melting point of crystalline boron (2350 K) at approximately 130 ms, subsequently approaching and eventually matching the temperature in air. Argon, serving as an inert control atmosphere, exhibits significantly lower overall particle temperatures due to the lack of exothermic reactions, and the temperature curve shows relatively greater noise due to weaker thermal radiation signals.

It is noteworthy that the timing of the peak particle surface temperature is closely related to the transition of combustion stages. In a steam atmosphere, the temperature reaches its maximum at approximately 200 ms, which corresponds to the middle and late stages of micro-explosive combustion. In air, the temperature peak occurs earlier (around 110 ms), also corresponding to the active period of micro-explosive combustion. This indicates that the micro-explosion stage is not only accompanied by dramatic structural changes and material ejection but also represents the period of strongest reactions on both the internal and external surfaces of the particle, where heat release is most concentrated. Upon entering the quasi-steady combustion stage, as the internal pores essentially disappear and the reaction surface area decreases, the particle surface temperature exhibits a slow declining trend.

After the laser irradiation stops, the particle surface temperature decays rapidly. The temperature decreases more slowly in a steam atmosphere, and the flameout time is longer, further confirming that steam helps sustain surface reactions at lower temperatures and prolongs self-sustaining combustion.

It should be noted that the temperature measurement method based on spontaneous emission spectra has a decreased signal-to-noise ratio at lower temperatures, which may affect the accuracy of temperature inversion. Therefore, temperature data from the initial heating stage are not included in Fig. 10, and the temperatures in argon also exhibit considerable fluctuations. However, during the main combustion stage, this method can reliably reflect the relative trend of particle surface temperature changes, providing a basis for understanding the combustion kinetics of boron particles.

3.3. Combustion mode and kinetic analysis

To quantitatively characterize the reaction rate of boron agglomerates at different combustion stages and reveal their controlling mechanisms, this section analyzes the particle size evolution data obtained from experiments based on the classical D^2 law for particle combustion, clarifying the combustion kinetic modes at different stages. Although the classical D^2 law was originally formulated for purely gas-phase diffusion-controlled combustion of homogeneous liquid droplets, its extension to the analysis of the diffusion-controlled combustion stage of boron and metal particles is well supported by theoretical developments and established literature (Hussmann & Pfitzner, 2010; Yeh & Kuo, 1996). During the quasi-steady combustion stage, the internal pores of the particle have largely disappeared, the surface oxide layer has been removed, and the particle assumes a nearly spherical, fully or partially molten morphology. Under these conditions, applying the D^2 law to analyze the combustion mode is physically justified. Assuming a spherical boron particle, the mass and combustion rate of the particle can be expressed as:

$$m = \rho V = \rho\left(\frac{\pi}{6}\right)D^3 \tag{3}$$

$$\frac{\mathrm{d}m}{\mathrm{d}t} = \frac{\pi}{4}\rho D\frac{\mathrm{d}D^2}{\mathrm{d}t} \tag{4}$$

where ρ is the particle density, and D is the particle diameter. Under diffusion control, the combustion rate is entirely determined by the diffusion rate. According to Fick's law, it can be readily deduced that the mass combustion rate is proportional to the particle diameter, thus:

$$-\frac{\mathrm{d}m}{\mathrm{d}t} = kD \tag{5}$$

where k is a proportionality constant. Combining (4) and (5), we obtain:

$$\frac{\mathrm{d}D^2}{\mathrm{d}t} = -\frac{4k}{\pi\rho} \tag{6}$$

Therefore, if the combustion mode of the boron particle is diffusion-controlled, D^2 decreases linearly with time. Defining the burning rate constant $\beta = 4k/\pi\rho$, integration yields:

$$D^2(t) = D_0^2 - \beta t \tag{7}$$

where D_0 is the initial diameter. By performing a linear fit to the data in the linear stage, the absolute value of the slope of the obtained line is the burning rate constant β. β is an intrinsic parameter characterizing the combustion characteristics of a specific fuel-oxidizer combination under given environmental conditions. A larger β value indicates faster combustion. This linear relationship suggests that the combustion process at this stage is relatively stable, and the local environment surrounding the particle (ambient temperature, oxidizer concentration, etc.) is also relatively stable. Although the particle shrinks, the entire diffusion and reaction fields can adjust rapidly enough to maintain a linear change in D^2. The disruption of this linear relationship signifies the end of quasi-steady combustion or a transition in the combustion mechanism.

Fig. 11 shows the D^2 variation curve of a boron agglomerate in steam. Analysis reveals that there are two approximately linear intervals before and after the micro-explosive combustion stage (with coefficient of determination $R^2 > 0.9$). The slopes of these two linear intervals differ significantly, corresponding to two combustion processes with distinctly different kinetic characteristics. The first linear stage (pre-micro-explosion) corresponds to the molten collapse stage described in Section 3.1.1. In this stage, D^2 decreases linearly with time, and the absolute value of the slope is large (denoted as β_1), indicating a very rapid size reduction. However, this sharp volume decrease primarily results from the molten collapse of the porous structure, rather than the oxidative consumption of boron. Therefore, although it conforms to the linear relationship of D^2, its physical essence is not diffusion-controlled combustion, but rather a physical melting and structural densification

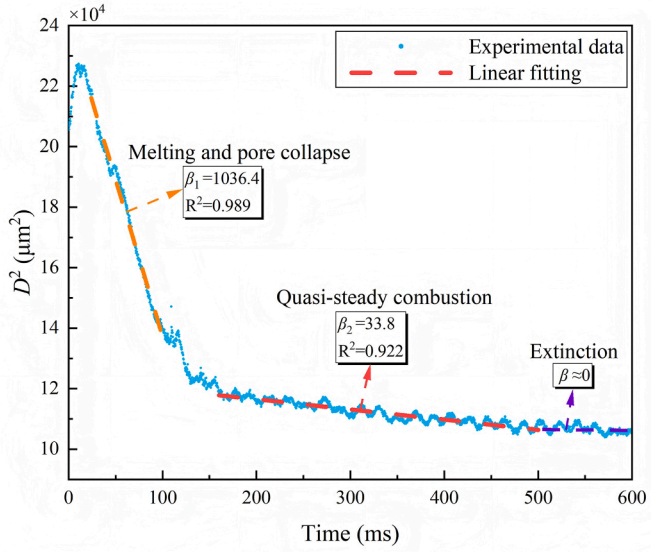

Fig. 11. The D^2 versus time and corresponding linear correlation in steam.

process dominated by heat transfer.

The second linear stage (post-micro-explosion) corresponds to the quasi-steady combustion stage described in Section 3.1.2. At this point, micro-explosions have ceased, and the internal pores of the particle have essentially disappeared. The particle structure at this stage consists of a surface-molten, nearly solid pure boron particle, similar to conventional boron particles, allowing analysis based on classical boron combustion theories. In this stage, D^2 also exhibits a good linear decay, with the absolute value of its slope denoted as β_2. This linear decay relationship indicates that the combustion process is controlled by a diffusion mechanism. The diffusion rate of the oxidant to the particle surface becomes the limiting step. After the laser stops, combustion gradually ceases, and the decreasing trend of D^2 gradually flattens ($\beta \rightarrow 0$).

The trend of D^2 variation in air is similar to that in steam, also exhibiting a linear change during the quasi-steady combustion stage, indicating that there is no essential difference in the particle combustion mode between the two atmospheres. The average burning rate constants β_1 and β_2 calculated for different atmospheres are shown in Fig. 12. During the quasi-steady combustion stage, the β_2 values in steam and air are of the same order of magnitude and relatively close, whereas β_2 in argon is near zero due to the absence of sustained oxidation reactions. This indicates that under diffusion-controlled combustion mode, steam as an oxidizer has comparable efficacy to air (despite its lower oxygen mole fraction). During the melting and pore collapse stage, the strong exothermic reaction in air leads to a faster particle melting rate, consequently resulting in the largest β_1 value in air.

3.4. Relative volume change and combustion efficiency

To quantitatively evaluate the overall reaction degree and fuel utilization efficiency of boron agglomerates in different oxidizing atmospheres, this section systematically analyzes the volume evolution throughout the combustion process based on the particle projected area sequence obtained from high-speed shadowgraph imaging, and proposes a method for calculating combustion efficiency based on inert atmosphere control experiments.

The instantaneous volume V of the particle during combustion is calculated from its projected area A, assuming the particle is spherical, giving $V = k \cdot A^{3/2}$, where k is the shape factor. The relative volume change is defined as:

$$\theta_V = \frac{V - V_0}{V_0} \times 100\% \tag{8}$$

In this equation, V_0 represents the initial particle volume prior to laser ignition. By tracking the variation of θ_V over time, the physical morphological changes and material consumption of the particle at different combustion stages can be directly visualized. Fig. 13 presents the average relative volume change of boron agglomerates in different atmospheres. The most pronounced volume reduction is observed in all atmospheres within the first 0–100 ms, which roughly corresponds to the pore collapse process during the preheating/ignition stage. The relative volume change is similar across the three atmospheres and is all lower than the particle porosity, indicating that the volume reduction at this stage primarily results from the collapse of internal pores within the boron agglomerate. Furthermore, the particle is not completely molten by the end of this stage, with some pores remaining inside. Additional volume loss occurs in steam and air between 100 and 200 ms, approximately corresponding to the micro-explosive combustion stage. The rate of volume reduction slows down during 200–500 ms, although continuous consumption persists in oxidizing atmospheres. By the end of the laser irradiation period (500 ms), the overall volume change rates in air and steam eventually converge to similar values (approximately 62%). The volume change rate in argon (38.3%) is close to the initially measured porosity (48.9% ± 5%), with the change occurring predominantly before 100 ms. This confirms that volume reduction in an inert atmosphere arises almost exclusively from physical melting and collapse, without net consumption of the boron. In contrast, the additional volume loss observed in reactive atmospheres can be attributed to the combustion consumption of boron itself.

To isolate the influence of physical changes and quantitatively evaluate the degree of chemical conversion of boron agglomerates, this paper proposes a reference experiment-based method for calculating combustion efficiency. The core idea is to use argon experiments to calibrate for physical volume shrinkage. The initial porosity of the boron agglomerate is defined as:

$$\varepsilon = 1 - \frac{V_{\text{solid}}}{V_0} \tag{9}$$

In the equation, V_{solid} represents the sum of the solid volumes of all the initial boron microspheres constituting the agglomerate (i.e., the volume of pure boron without pores). In argon, it is assumed that the volume reduction is entirely caused by pore collapse, with no consumption of the boron substrate, meaning the combustion efficiency is 0. Therefore, the particle volume after laser heating in argon can be approximately regarded as the volume of the pure boron condensed-phase material after the removal of initial pores, i.e., $V_{\text{solid}} \approx V_{\text{Ar}}$. From this, the porosity of the boron agglomerate can be estimated. The combustion

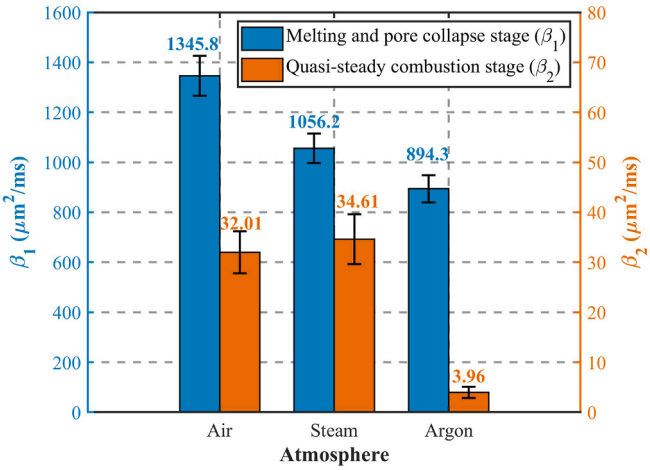

Fig. 12. Burning rate constants in different atmospheres.

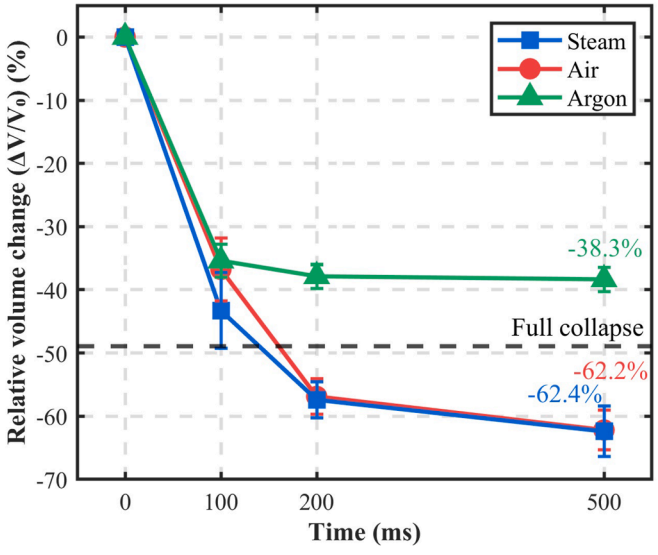

Fig. 13. Average relative volume change of boron agglomerates in different atmospheres.

efficiency η_c of the boron agglomerate in a reactive atmosphere can be defined as the percentage of consumed boron volume relative to the initial solid boron volume, calculated using the following formula:

$$\eta_c = \frac{V_{solid} - V_{end}}{V_{solid}} \times 100\% \quad (10)$$

Alternatively, expressed in terms of relative volume change and porosity, it can be written as:

$$\eta_c = \frac{-\theta_{V,end} - \varepsilon}{1 - \varepsilon} \quad (11)$$

Here, V_{end} is the final volume after experiment (after particle cooling), and $\theta_{V,end}$ is the corresponding relative volume change. The core idea of this method lies in using the argon experiment to calibrate for the same physical shrinkage process, thereby isolating the "combustion consumption" component from the total volume change observed in reactive atmospheres. This effectively avoids errors introduced by the difficulty of precisely determining the particle porosity after the reaction. It should be noted that the exothermic chemical reactions in air and steam elevate the particle temperature, which may render the molten collapse more rapid and complete than in the inert argon atmosphere, thereby slightly overestimating the chemical consumption. Nevertheless, after sufficient heating for 500 ms, the volume change curves in all 3 atm have largely plateaued, indicating that physical densification is nearly complete and that differences in thermal history exert only a limited influence on the final volume. While not absolutely precise, this method provides a practical and reasonable benchmark for comparative evaluation of combustion efficiency across different atmospheres.

Applying the above formula, the combustion efficiencies in air and steam are calculated to be 38.7% and 39.1%, respectively. The proximity of these values indicates that, under the present experimental conditions, the two oxidizing atmospheres achieve comparable levels of boron fuel utilization. This finding corroborates the similar burning rate constants observed during the quasi-steady combustion stage in Section 3.3. The vigorous ejection phenomena in steam are more conducive to particle dispersion, whereas the stronger exothermic reaction in air promotes faster melting and pore collapse in the early stage. The combined effects of these two mechanisms ultimately lead to the convergent combustion efficiencies.

3.5. Structural evolution process of boron agglomerates in steam

Based on the above experimental results and classical boron ignition and combustion theories, this section proposes a physicochemical model for the steam environment to elucidate the complete structural evolution process and underlying mechanisms of boron agglomerates from melting and pore collapse to micro-explosion combustion. The core of this process lies in the formation of a layered structure from the surface inward under the combined effects of environmental heating and reaction heat, ultimately triggering micro-explosions due to internal pressure accumulation.

In the initial stage of laser heating, the particle surface temperature rapidly exceeds the melting point of boron oxide (B_2O_3, 723 K). Boron microparticles can dissolve into the molten B_2O_3, generating a glassy intermediate oxide $(BO)_n$, which diffuses outward and volatilizes at the oxide layer surface. Simultaneously, molten boron oxide can also directly evaporate (Feng et al., 2025; Liang et al., 2021).

$$2/3B(s) + 2/3B_2O_3(l) \rightarrow 2/n(BO)_n(l) \quad (R1)$$

$$2/n(BO)_n(l) \rightarrow B_2O_2(g) \quad (R2)$$

$$B_2O_3(l) \rightarrow B_2O_3(g) \quad (R3)$$

At this stage, the pores on the surface and within the boron agglomerate have not yet completely closed. H_2O can diffuse inward through these pores and react with the internal boron microparticles. The gaseous products generated from the reactions and volatilization can be discharged through the pores. On one hand, H_2O can react with $(BO)_n$ that has diffused to the oxide layer surface, further oxidizing it (Yeh & Kuo, 1996; Liang et al., 2021). These reactions can be represented as R4–R8, with the overall reaction being GR1.

$$H_2O(g) \rightarrow H(a) + OH(a) \quad (R4)$$

$$1/n(BO)_n(l) + OH(a) \rightarrow HBO_2(g) \quad (R5)$$

$$HBO_2(g) \rightarrow H(a) + BO_2(g) \quad (R6)$$

$$1/n(BO)_n(l) + BO_2(g) \rightarrow B_2O_3(l) \quad (R7)$$

$$2H(a) \rightarrow H_2(g) \quad (R8)$$

$$2/n(BO)_n(l) + H_2O(g) \rightarrow B_2O_3(l) + H_2(g) \quad (GR1)$$

On the other hand, H_2O can diffuse inward through the liquid oxide layer and directly react with boron on the inner surface of the oxide layer (Gaponenko et al., 1981). These reactions can be represented as R9–R10, which, together with R8, constitute the overall reaction GR2.

$$3/2H_2O(g) + 3/2B_2O_3(l) \rightarrow 3HBO_2(a) \quad (R9)$$

$$B(s) + 3HBO_2(a) \rightarrow 2B_2O_3(l) + 3H(a) \quad (R10)$$

$$B(s) + 3/2H_2O(g) \rightarrow 1/2B_2O_3(l) + 3/2H_2(g) \quad (GR2)$$

The above reactions oxidize boron, producing boron oxide and hydrogen, which thickens the oxide layer and releases heat, thereby accelerating particle melting. Furthermore, water vapor can react with B_2O_3 to form gaseous products such as HBO_2 (R11, R12), which accelerates the removal of the oxide layer (Wahbeh et al., 2012).

$$B_2O_3(l) + H_2O(g) \rightarrow 2HBO_2(g) \quad (R11)$$

$$B_2O_3(l) + 3H_2O(g) \rightarrow 2H_3BO_3(g) \quad (R12)$$

It should be noted that the reaction mechanism described above is inferred primarily from experimental studies on boron-water reactions reported in the literature (Wahbeh et al., 2012, 2013) and from thermodynamic analyses. In addition, preliminary reactive force field molecular dynamics (ReaxFF-MD) simulations conducted in this work corroborate that H_2 and HBO_2 are the dominant gaseous products of the high-temperature boron-water reaction (see Section S5 in the Supplementary Material). Direct in-situ detection of gaseous products from single-particle combustion awaits future improvements to the experimental system.

From the perspective of heat and mass transfer characteristics of the boron agglomerate, the large particle size and porous structure result in a high Biot number ($Bi = hL_c/k$), indicating significant internal thermal conduction resistance. Consequently, heat tends to accumulate in the surface layer, promoting the initial formation of a continuous molten boron-boron oxide mixed layer on the surface. Simultaneously, the high mass transfer Biot number ($Bi_m = k_m L_c/D_{eff}$) indicates that the diffusion of water vapor toward the particle core is limited. Before the surface layer melts and seals, water vapor primarily diffuses through pores into the near-surface region of the particle to participate in reactions. As a result, the particle surface layer maintains a higher temperature, with faster melting and reaction rates, and the molten layer propagates inward from the exterior.

Under the action of surface tension in the molten layer, boron microparticles coalesce, pores collapse, and the particle volume decreases. As the molten layer advances inward, the surface ultimately forms a dense film that seals the surface pores, preventing material exchange between the interior and exterior. This results in the formation of a "core-shell" layered structure characterized by a sealed surface layer with residual pores remaining in the interior.

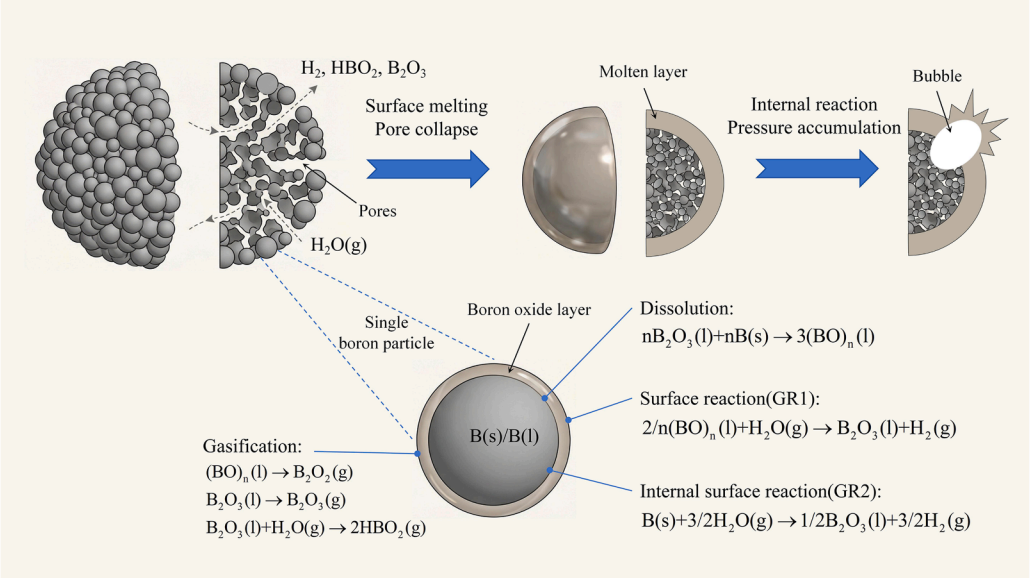

Fig. 14. Structural evolution model of boron agglomerates in steam.

After the surface layer is sealed, the interior of the particle becomes a semi-confined reaction space. The water vapor that diffused into the internal pores prior to sealing continues to react with the inner-surface boron at high temperatures, generating gaseous products such as H_2 and HBO_2 while releasing heat, leading to a sharp rise in both temperature and pressure. Due to the sealing effect of the outer shell, the internal pressure continuously accumulates. When the internal pressure exceeds the mechanical strength of the thin shell, the shell ruptures locally. Thus, it can be seen that the occurrence of micro-explosions requires the simultaneous fulfillment of two fundamental conditions: the melting and sealing of the particle surface layer, and the accumulation of pressure from internally generated gases.

The steam environment is characterized by efficient oxide layer removal but relatively weak exothermic reactions, resulting in the formation of a thinner surface molten layer. Concurrently, the high gas production rate of the boron-water reaction allows high-temperature gases, molten droplets, and unreacted boron microparticles to be continuously ejected from a fixed rupture site, forming the typical micro-explosion mode of "weak expansion but strong ejection" observed in the experiments.

Fig. 14 comprehensively illustrates the above process. Based on the boron-water chemical reaction mechanism and the structural evolution of boron agglomerates, this model reveals the key pathways of boron agglomerate combustion in steam. It should be acknowledged that the laser heating employed in this study is directional, which differs from the omnidirectional heating conditions in an actual engine. Nevertheless, after a brief preheating period, a dense molten layer can also form on the side opposite to the laser irradiation (see Section S4 in the Supplementary Material). Under the omnidirectional heating conditions encountered in practical applications, surface sealing would likely occur earlier and micro-explosions might be triggered slightly sooner; however, the fundamental micro-explosion mode and the characteristic structural evolution of the particle are expected to remain unchanged.

4. Conclusions

This study systematically investigated the combustion process of boron agglomerates in pure steam using a laser ignition single-particle experimental system. The results reveal that the combustion of boron agglomerates in steam exhibits distinct stage characteristics. Steam not only acts as an effective oxidizer supporting vigorous boron combustion but also induces physical changes such as sustained ejection-type micro-explosions through its unique chemical reaction characteristics (accelerating oxide layer removal to generate HBO_2 and producing H_2), significantly altering the combustion process and forming a micro-explosion mode different from the periodic expansion observed in air. The D^2 analysis indicates that the combustion mode of boron agglomerates is diffusion-controlled after the conclusion of micro-explosions. Based on this, a double-film model with intermediates such as HBO and BO can be established to quantitatively describe the combustion process of boron particles in steam. However, further microscopic mechanism studies, such as molecular dynamics simulations and product detection, are needed to investigate the specific reaction pathways. Despite differences in reaction pathways, the pure steam environment ultimately achieved a combustion efficiency comparable to that in low-concentration oxygen. Notably, the steam environment exhibited advantages under lower temperature conditions (during the initial ignition stage and after laser cutoff), confirming the potential of boron for efficient energy release in steam. These findings provide critical data supporting the feasibility of applying boron-based fuels in water ramjet.

CRediT authorship contribution statement

Gan Yang: Writing – original draft, Software, Investigation. **Binbin Chen:** Writing – review & editing, Validation. **Likun Ma:** Funding acquisition, Conceptualization. **Yunchao Feng:** Data curation. **Lian Duan:** Methodology. **Zhixun Xia:** Funding acquisition. **Chaolong Li:** Project administration.

Declaration of competing interest

The authors declare that they have no known competing financial interests or personal relationships that could have appeared to influence the work reported in this paper.

Acknowledgement

This work was supported by the National Natural Science Foundation of China (Grant No. 12502325) and the Innovation Research Foundation of National University of Defense Technology (Grant No. ZK24-62 and No. 25-ZZCX-DFXJS-05).

Appendix A. Supplementary data

Supplementary data to this article can be found online at https://doi.org/10.1016/j.partic.2026.05.007.

References

Brown, R. C., Kolb, C. E., Rabitz, H., Cho, S. Y., Yetter, R. A., & Dryer, F. L. (1991). Kinetic model of liquid B2O3 gasification in a hydrocarbon combustion environment: I. Heterogeneous surface reactions. *International Journal of Chemical Kinetics, 23*(11), 957–970. https://doi.org/10.1002/kin.550231102

Duan, L., Xia, Z., Feng, Y., Chen, B., Ma, L., & Hu, J. (2024a). Transient flameout process of boron-magnesium agglomerates during combustion in oxygen-rich atmospheres. *Particuology, 88*, 290–301. https://doi.org/10.1016/j.partic.2023.10.002

Duan, L., Xia, Z., Feng, Y., Chen, B., Zhang, J., Ma, L., & Hu, J. (2024b). Formation of bubbles and microexplosions in burning boron agglomerates. *Combustion and Flame, 264*, Article 113432. https://doi.org/10.1016/j.combustflame.2024.113432

Duan, L., Xia, Z., Feng, Y., Chen, B., Zhang, J., Ma, L., & Huang, L. (2023). Thermal behavior and laser-induced heating characteristics of boron agglomerates in various atmospheric conditions. *Journal of Thermal Analysis and Calorimetry, 148*(23), 13629–13638. https://doi.org/10.1007/s10973-023-12638-8

Feng, Y., Hu, Z., Liu, J., Tang, Y., Zhao, M., & Shi, B. (2025). Numerical study on the ignition and flame propagation of micron-sized boron particles in the O2-H2O-N2 atmosphere. *Aerospace Science and Technology, 158*, 109877. https://doi.org/10.1016/j.ast.2024.109877

Gaponenko, L. A., Biunovskii, S. N., Tulupov, Y. I., & Yakovleva, T. A. (1981). A model for the ignition of a single boron particle in a medium containing water. *Combustion, Explosion and Shock Waves, 17*(1), 9–14. https://doi.org/10.1007/BF00772774

Hussmann, B., & Pfitzner, M. (2010a). Extended combustion model for single boron particles – Part I: Theory. *Combustion and Flame, 157*(4), 803–821. https://doi.org/10.1016/j.combustflame.2009.12.010

Hussmann, B., & Pfitzner, M. (2010b). Extended combustion model for single boron particles – Part II: Validation. *Combustion and Flame, 157*(4), 822–833. https://doi.org/10.1016/j.combustflame.2009.12.009

Liang, D., Liu, J., Zhou, Y., Zhou, J., & Cen, K. (2018). Ignition delay kinetic model of boron particle based on bidirectional diffusion mechanism. *Aerospace Science and Technology, 73*, 78–84. https://doi.org/10.1016/j.ast.2017.11.044

Liang, D., Shen, D., Zhong, W., Wang, Y., & Liu, J. (2021). Nuclear shell model for the ignition process of boron particle with binary surface oxide layer. *Combustion and Flame, 225*, 320–328. https://doi.org/10.1016/j.combustflame.2020.11.008

Liu, S., Han, L., Liu, H., Song, Y., Liu, L., & Hu, S. (2024). Experimental and numerical study on ignition and combustion characteristics of boron-magnesium composite powders. *Particuology, 84*, 12–29. https://doi.org/10.1016/j.partic.2023.02.012

Majji, M., Abzal, S., Jacob, N., Maiti, P., Choppella, S., Ravva, M. K., Maram, P. S., Ghosh, S., Dash, J. K., & Motapothula, M. (2024). Efficient photocatalytic green hydrogen production using crystalline elemental boron nanostructures under visible light. *International Journal of Hydrogen Energy, 56*, 338–347. https://doi.org/10.1016/j.ijhydene.2023.12.113

Meera, M. S., Sasidharan, S. K., Hossain, A., Kiss, J., Kónya, Z., Elias, L., & Shibli, S. M. A. (2022). Effect of excess B in Ni_2 P-Coated boron nitride on the photocatalytic hydrogen evolution from water splitting. *ACS Applied Energy Materials, 5*(3), 3578–3586. https://doi.org/10.1021/acsaem.1c04086

Mi, X., Goroshin, S., Higgins, A. J., Stowe, R., & Ringuette, S. (2013). Dual-stage ignition of boron particle agglomerates. *Combustion and Flame, 160*(11), 2608–2618. https://doi.org/10.1016/j.combustflame.2013.06.004

Qu, Y., Xia, Z., Na, X., Ma, L., Feng, Y., Chen, B., & Zhang, J. (2025). Primary combustion and near-burning surface conglomeration characteristics of boron-containing fuel-rich propellant. *Combustion and Flame, 274*, Article 114040. https://doi.org/10.1016/j.combustflame.2025.114040

Rohani, P., Kim, S., & Swihart, M. T. (2016). Boron nanoparticles for room-temperature hydrogen generation from water. *Advanced Energy Materials, 6*(12), Article 1502550. https://doi.org/10.1002/aenm.201502550

Rosenband, V., Gany, A., & Timnat, Y. M. (1998). Magnesium and boron combustion in hot steam atmosphere. *Defence Science Journal, 48*(3), 309–315. https://doi.org/10.14429/dsj.48.3953

Song, Q., Cao, W., Wei, X., Liu, J., Yuan, J., Li, X., Guo, X., & Gao, D. (2021). Laser ignition and combustion characteristics of micro- and nano-sized boron under different atmospheres and pressures. *Combustion and Flame, 230*, Article 111420. https://doi.org/10.1016/j.combustflame.2021.111420

Vishnevetsky, I., Epstein, M., Abu-Hamed, T., & Karni, J. (2008). Boron hydrolysis at moderate temperatures: First step to solar fuel cycle for transportation. *Journal of Solar Energy Engineering, 130*(1), Article 014506. https://doi.org/10.1115/1.2807215

Wahbeh, B., Hamed, T. A., & Kasher, R. (2012). Hydrogen and boric acid production via boron hydrolysis. *Renewable Energy, 48*, 10–15. https://doi.org/10.1016/j.renene.2012.04.043

Wahbeh, B., Tell, S., Abu Hamed, T., & Kasher, R. (2013). Kinetics of boron hydrolysis for hydrogen production. *International Journal of Hydrogen Energy, 38*(14), 6210–6214. https://doi.org/10.1016/j.ijhydene.2012.12.124

Wu, X., & Wei, Z. (2024). Multiphase ignition and combustion model and its characteristics of boron particles based on dynamic experimental phenomena. *Combustion and Flame, 265*, Article 113445. https://doi.org/10.1016/j.combustflame.2024.113445

Yeh, C. L., & Kuo, K. K. (1996). Ignition and combustion of boron particles. *Progress in Energy and Combustion Science, 22*(6), 511–541. https://doi.org/10.1016/S0360-1285(96)00012-3

Zhang, T., Song, F., Qian, Y., Gao, H., Shaw, J., & Rao, Y. (2021). Elemental engineering of high-charge-density boron in nickel as multifunctional electrocatalysts for hydrogen oxidation and water splitting. *ACS Applied Energy Materials, 4*(6), 5434–5442. https://doi.org/10.1021/acsaem.0c03179